RESEARCH ARTICLE

3-D Printable Metal-Dielectric Metasurface for Risley Prism-Based Beam-Steering Antennas

MD YEAKUB ALI [1], **(Student Member, IEEE), ALI LALBAKHSH** [1], **(Senior Member, IEEE),**
KHUSHBOO SINGH [2], **(Member, IEEE), SLAWOMIR KOZIEL** [3,4], **(Fellow, IEEE),**
AND LUKASZ GOLUNSKI [4]

[1] School of Engineering, Macquarie University, Sydney, NSW 2109, Australia
[2] School of Electrical and Data Engineering, University of Technology Sydney (UTS), Sydney, NSW 2007, Australia
[3] Department of Engineering, Engineering Optimization and Modeling Center, Reykjavik University, 102 Reykjavik, Iceland
[4] Faculty of Electronics, Telecommunications, and Informatics, Gdańsk University of Technology, 80-233 Gdańsk, Poland

Corresponding authors: Md Yeakub Ali (mdyeakub.ali@students.mq.edu.au) and Ali Lalbakhsh (ali.lalbakhsh@mq.edu.au)

ABSTRACT A 3-D printable, planar, metal-dielectric metasurface-based, 2-D beam-steering system for aperture-type antennas is presented in this paper. This beam-steering system, also known as the near-field meta-steering system, comprises two fully passive phase-gradient metasurfaces placed in the antenna's near-field region to steer the radiation beam. To address the non-uniform electric field phase of the aperture antenna, phase correction is also incorporated into the bottom metasurface placed on top of the antenna aperture in its near-field to enhance the far-field radiation of the antenna. Near-field phase transformation and phased array antenna theory concepts are applied to design the proposed metasurfaces. Two types of metal-dielectric unit cells are implemented to provide a phase range of 360°. The height of each metasurface is only 6.25 mm ($0.25\lambda_0$), and the height of the whole system is only $1.56 \lambda_0$ at 12 GHz. The proposed beam-steering system with a resonant cavity antenna can steer the beam to a maximum of $\pm44°$ in the elevation plane and 360° in the azimuth plane with only a 1.4 dB (17 dB - 15.6 dB) deviation in directivity over the full steering range.

INDEX TERMS 3-D printing, beam-steering, metasurface, near-field phase transformation, near-field meta-steering, resonant cavity antenna, transmission phase delay.

I. INTRODUCTION

A low-cost and efficient beam-steering system is one of the most researched topics in wireless communication, especially for the latest technologies like 5G [1] and satellite communications [2]. In applications where the transmitter or receiver is on moving platforms, beam steering plays a significant role in uninterrupted data connectivity, minimizing interference and signal attenuation [3].

Beam steering systems can be categorized based on their steering mechanism as mechanical [4], electronic [5], or hybrid [6]. While mechanical systems offer extensive beam scanning capabilities, their complexity and weight

The associate editor coordinating the review of this manuscript and approving it for publication was Zahra Shaterian .

make them costly and bulky due to the intricate rotation mechanisms of the antenna. On the other hand, although faster, compact, and more efficient, electronic systems have limited scanning ranges, are expensive due to the requirement for numerous phase shifters, and suffer from high losses in the complex feed circuitry. Hybrid systems combine aspects of both approaches [7].

In the last few years, one approach has gained significant interest for steering the beam of a radiating source using passive phase-gradient metasurfaces placed in the near-field region of a radiating source. A metasurface, a 2-D meta-material, is an artificially engineered periodic structure with special electromagnetic characteristics that are not achievable in materials from nature [8], [9]. Recently, metasurfaces are realized to enhance far-field radiation, improve operational

bandwidth and efficiency, convert polarization, and beam tilting of antennas [1], [10], [11], [12], [13], [14], [15], [16]. The beam steering system utilizing phase-gradient metasurface is known as a near-field meta-steering system, and the metasurfaces for beam steering are developed following the principle of the Risely prism in optics [17], [18]. The phase delay gradient of the metasurface is constant along the y-axis and variable along the x-axis. In this approach, two phase-gradient metasurfaces are placed in front of the base antenna and rotated around the antenna axis independently or synchronously to rotate the beam of the radiating source in both the azimuth and elevation plane [19].

The meta-steering structures may be dielectric [2], [20], metallic [21], [22], or composite [17], depending on the material used. A metasurface consists of a printed patch on a dielectric substrate that needs multi-layers to provide a 360° phase range. Substrate laminates are expensive and need special machining to bond multi-layers. Only dielectric structures fabricated by conventional subtractive manufacturing (SM) are created from the dielectric block. A stepped dielectric (SD) and dielectric wedge (DW) structure-based beam steering system is proposed in [23]. SD and DW are produced from a block of dielectric material using subtractive manufacturing. The problem with this type of structure is the phase wrapping points [18]; one edge of the structure is so thin that it makes the design structurally weak. A perforated dielectric-based meta-steering system is reported in [1]. The metasurfaces from dielectric laminates were fabricated using a conventional subtracting drilling process. Also, the structure is prone to breakage as it becomes fragile due to perforation. The dielectric materials are expensive, and the subtractive process causes material waste. Additive manufacturing, or 3-D printing, eliminates the above-mentioned limitations associated with traditional subtractive manufacturing and provides enormous flexibility for any tailored design. Compared to traditional manufacturing, 3-D printing has many advantages, including low production cost, rapid prototyping, the ability to fabricate customized and multi-material structures, and error detection capability before final realization [24].

In 3-D printed metasurface design, the choice of material has a significant role in their overall profile and performance. 3-D printed metasurfaces designed using conventional materials like acrylonitrile butadiene styrene (ABS) or polylactic acid (PLA) have a higher profile due to the limited permittivity (2.5-2.8) of the materials. For example, a 3-D printed stepped dielectric- and dielectric wedge-based beam steering system consisting of PLA material is reported in [2]. The height of this phase gradient structure is 3.1 λ_0, and it is non-planar, suffering from shadowing issues. In [25], the authors proposed a 3-D printed perforated metasurface with ABS material for antenna beam steering, but the height of the metasurface is $1.76\lambda_0$, which is considerably high. Using RF-graded dielectric with low loss and higher permittivity improves the performance and helps to develop a low-profile structure. A metal-dielectric 3-D printable metasurface-based

beam steering system using PREPERM® ABS 1000 ($d_k = 10$) [26] is proposed in [27] with metasurface height 0.36 λ_0. However, it suffers from shadowing effects due to its non-planar structure.

This paper presents a metal-dielectric, phase-gradient, metasurface-based beam steering system with a resonant cavity antenna. The height of each metasurface is lower than that of its counterparts, as reported in the literature and designed to steer the antenna beam. Two types of unit cells, each consisting of metal and dielectric, have been utilized to design the highly transparent hybrid metasurfaces to achieve a wider transmission phase coverage up to 360°. The height of the proposed metasurface is 6.25 mm (0.25 λ_0), which is 30%, 85%, and 92% lower than the structures reported in [2], [25] and [27], respectively. Additionally, the metasurface is highly transparent, with a transmission magnitude of 2.1 dB for all constituent unit cells. Instead of conventional 3-D printing materials like ABS or PLA, RF-graded commercially available dielectric material, PREPERM® ABS filament with $d_k = 4.4$ has been chosen for fabrication. In particular, the proposed design offers advantages over existing metasurface-based beam-steering systems by providing a more compact and lightweight solution through the use of comparatively thinner metasurfaces with holes. Additionally, the use of metal-dielectric 3-D printing technology simplifies the manufacturing process and opens new avenues for further research in electromagnetic surface technologies. The beam steering surfaces are planar and do not have shadowing problems like DW or SD. Moreover, the directivity deviation is only 1.4 dB at 12 GHz within the full beam steering range for different angles of rotation of the steering surfaces. Using unit cells with through holes also reduces the overall weight of the antenna system, increasing its power efficiency. This type of beam-steering antenna solution can be used as compact data download terminals and can be installed on rooftops along with a battery and solar panel for autonomous operation. Such a terminal can be installed on any moving platform and integrated with existing cellular networks via satellite using hybrid networks.

The other sections of this paper are organized as follows: the working principle of the near-field meta-steering system is elaborated in Section II. The design process of the proposed beam steering system is described in detail in Section III. The numerical results are analyzed in Section IV, and an evaluative summary is shown in Section V.

II. BEAM STEERING MECHANISM WITH METASURFACE

A schematic depiction of a near-field meta-steering system is illustrated in Fig. 1. It comprises a fixed-beam resonant cavity antenna (RCA) as an illuminating source and two phase-gradient metasurfaces atop it. Due to the non-uniform phase distribution in the near field of the RCA, the first metasurface over the antenna must compensate for the non-uniformity to enhance far-field radiation and create linear progressive phase delay to tilt the beam to an offset angle (δ_1), which is essentially the same as the
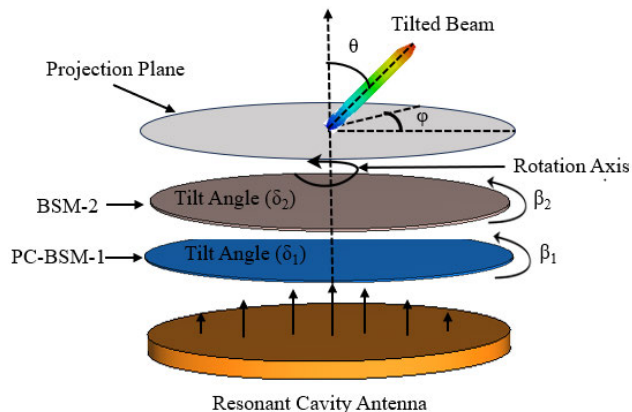
FIGURE 1. The schematic diagram of a beam-steering system with a pair of phase-gradient metasurfaces, rotating PC-BSM-1 and BSM-2, the beam direction is varied in the elevation and azimuth plane.

phase-gradient of the metasurface. This metasurface is called the phase-correction and beam-steering metasurface (PC-BSM-1). On the other hand, the upper metasurface only creates linear progressive phase delay and is referred to as the beam-steering metasurface (BSM-2). The beam of the base antenna can be tilted to any desired direction in both elevation and azimuth planes by co-rotating or counter-rotating the two metasurfaces independently or synchronously. The antenna beam can be steered in both planes by rotating either a single metasurface or both to different angles.

The direct relationship between the gradients of the two metasurfaces, their rotation angles, and the beam-steering angle can be visualized using the operating principles of a Risley prism. The fundamental concept of the Risley prism is explained in detail in [17] and [20]. The beam location in the far-field region is represented by the elevation angle (θ) and azimuth angle (ϕ). These two angles (θ and ϕ) depend on the rotation angles of the two metasurfaces and their individual beam-tilting angles. The rotation angles of the lower and upper metasurface are denoted by β_1 and β_2, respectively, and their corresponding individual beam tilting angles are represented by δ_1 and δ_2, respectively. The rotation of metasurfaces steers the antenna beam, whose location can be estimated using either the first-order paraxial approximation [28] or the phase method [29]. The first-order paraxial method is developed following the principle of the Risley prism. The detailed analytical elaboration of this method is presented in [28], and a brief overview is provided here. Beam steering direction (θ, ϕ) is calculated using the following equations [17]:

$$\theta = \sqrt{\delta_1^2 + \delta_2^2 + 2\delta_1\delta_2 cos(\beta_1 - \beta_2)} \quad (1)$$

$$\phi = \tan^{-1}\left(\frac{\delta_1 \sin \beta_1 + \delta_2 \sin \beta_2}{\delta_1 \cos \beta_1 + \delta_2 \cos \beta_2}\right) \quad (2)$$

In this work, both steering surfaces are designed to have the same phase gradient, and they can tilt a broadside beam to

the same offset angle, i.e., $\delta_1 = \delta_2 = \delta$. Thus, Eq. 1 and 2 can be written as below:

$$\theta = \sqrt{2\delta^2(1 + cos(\beta_1 - \beta_2)} \quad (3)$$

$$\phi = \tan^{-1}\left(\frac{\sin \beta_1 + \sin \beta_2}{\cos \beta_1 + \cos \beta_2}\right) \quad (4)$$

The phase method has been introduced more recently than the first-order paraxial method. In the phase method, the phase-delay gradient of the steering surface can be determined by the equations provided below [29]:

$$q_i = \sin \delta_i \times k_0, \quad (5)$$

where δ_i represents the individual beam tilting angle of the beam-steering metasurfaces and k_0 represents the free-space wave number at the design frequency. After calculating the phase gradient of each steering metasurface from Eq. 5, the beam direction angles can be calculated using the following equations,

$$\theta = \sin^{-1}\left[\frac{1}{k}\left[q_1^2 + q_2^2 + 2q_1q_2 \cos(\beta_1 - \beta_2)\right]^{1/2}\right] \quad (6)$$

$$\phi = \tan^{-1}\left(\frac{q_1 \sin \beta_1 + q_2 \sin \beta_2}{q_1 \cos \beta_1 + q_2 \cos \beta_2}\right) \quad (7)$$

Both metasurfaces implemented in this work are designed to tilt the beam to an offset angle of 22°, i.e., $\delta_1 = \delta_2 = 22°$. When the lower beam-steering metasurface is fixed, and the upper surface is rotated from 0° to 180° in anti-clockwise with a step size of 30°, the corresponding beam direction is calculated using both the first order paraxial method and phase method and listed in Table 1.

TABLE 1. Theoretically calculated beam-steering directions for the rotation of upper surface from 0° to 180° with a step size 30° when β_2=0°.

Orientation of Metasurfaces		First Order Paraxial Method		Phase Method	
β_1 (deg.)	β_2 (deg.)	θ (deg.)	ϕ (deg.)	θ (deg.)	ϕ (deg.)
0	0	44	0	48.52	0
0	30	42.5	15	46.35	15
0	60	38.1	30	40.45	30
0	90	31.11	45	31.99	45
0	120	22	60	22	60
0	150	11.39	75	11.18	75
0	180	0	90	0	90

III. BEAM-STEERING SYSTEM DESIGN

The proposed beam-steering system consists of a resonant cavity antenna, a phase-correcting and beam-steering metasurface, and a beam-steering metasurface. The design process of RCA and the metasurfaces is described in the following sections.

A. RESONANT CAVITY ANTENNA

The proposed metal-dielectric metasurface can be realized for any aperture-type antenna for beam-steering applications. A resonant cavity antenna has been utilized in this work

as a radiating source to demonstrate the proposed proto-type. The resonant cavity antenna configuration includes a ground plane, partially reflecting surface (PRS), and WR-75 waveguide to coax adaptor. The lateral dimensions of both the ground plane and the PRS are 100.8 mm × 100.8 mm ($\approx 4\lambda_0 \times 4\lambda_0$), where λ_0 represents the free-space wavelength at the design frequency (12 GHz). A metallic slot antenna excited with a WR-75 waveguide to coax adaptor is used as the base antenna. The slot in the ground plane is 13.5 mm long and 8.53 mm wide. The PRS comprises Rogers TMM 4 (D_k=4.7) dielectric material. An initial distance of 12.5 mm ($\approx \lambda_0/2$) between PRS and the ground plane is later strategically tuned to create a resonance between these two planes at the design frequency of 12 GHz, enhancing radiation performance. Due to the feeding position of the excitation source, the near-field phase distribution of RCA is non-uniform, resulting in poor far-field performance. Phase uniformity is enhanced using the near-field phase-correction method by implementing a combined phase-correcting and beam steering metasurface.

B. UNIT CELL ANALYSIS FOR METASURFACE DESIGN

The initial step in designing a metasurface involves analyzing the unit cell (UC), a fundamental building block of the metasurface [18], [30], [31]. The proposed highly transparent hybrid metasurface comprises two types of unit cells composed of dielectric material (with dielectric constant, d_k=4.4, and loss tangent, $\tan\delta$=0.004) and metal. Two types of unit cells are employed in developing the proposed metasurface to provide a complete transmission phase coverage from 0° to 360° while maintaining a lower profile and higher transmission magnitude, which is essential for beam steering applications. The lateral dimensions of the unit cell should be sub-wavelength size [32]. The height and lateral dimensions of the proposed unit cell are 6.25 mm ($\approx \lambda_0/4$) and 8.4 mm ($\approx \lambda_0/3$), respectively. The length and width of the unit cells are chosen following the unit cell analysis reported in [33], [34], and [35]. There are three metal layers in each unit cell: middle, bottom, and top. The thickness of the metal is 0.5 mm, the width of the metal layer of the inner arms is 1 mm, and the width of the metal surrounding the cell edge is 0.5 mm. The unit cell depicted in Fig. 2a without an air inclusion in
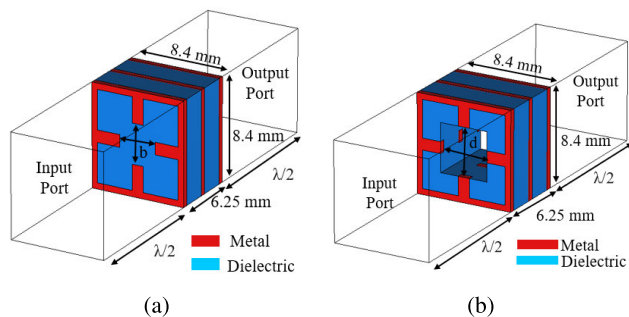
FIGURE 2. Unit cell (a) type-I (b) type-II.
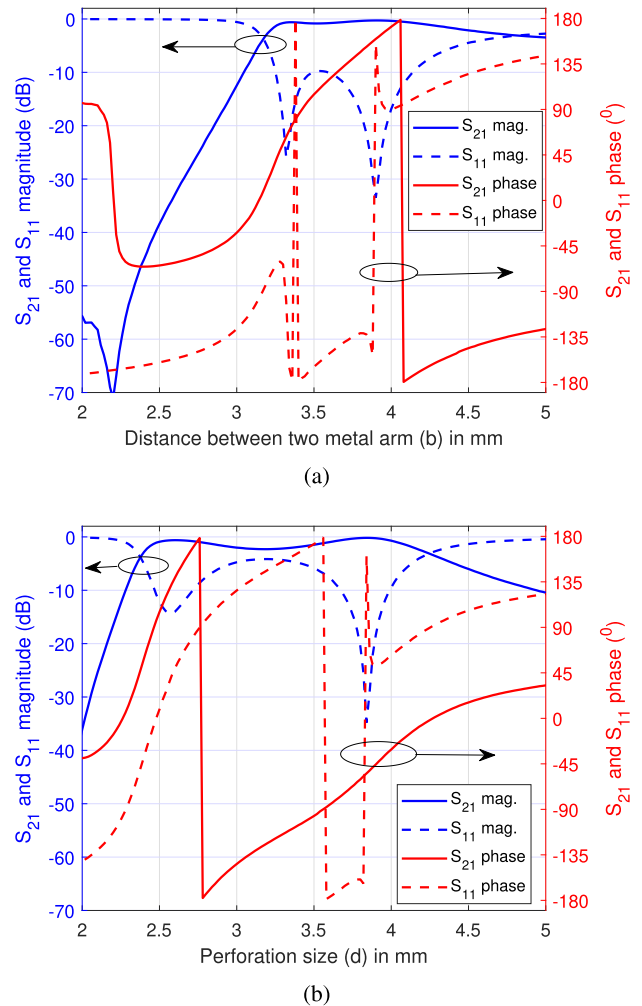
FIGURE 3. Transmission (S_{21}) and reflection (S_{11}) magnitude and phase of (a) UC type-I, with the variation of the gap between the inner arms, and (b) UC type-II, with the variation of air perforation size.

the center is referred to as UC type-I, while the one with an air inclusion (a through-hole) in the center, shown in Fig. 2b is referred to as UC type-II.

In the initial step of designing the metasurface, the unit cells are modeled in CST (computer simulation technology) Microwave Studio and analyzed under unit cell boundary conditions using floquet port analysis within the frequency domain solver. In UC type-I, the gap between the ends of the two inner arms, denoted as 'b,' and in UC type-II, the size of air gap inclusion, denoted as 'd', are varied to generate phase delays ranging between 0° to 360°. Using parametric sweep, the transmission (S_{21}) and reflection(S_{11}) magnitudes and phases are recorded in a database, and cells with the desired transmission characteristics are selected to design the proposed metasurface. The transmission magnitude and phase variations of UC type-I and UC type-II with respect to variations in 'b' and 'd' are shown in Fig. 3. The reflection characteristics are also included in the same figure.

TABLE 2. BSM-2 design: cell's location, progressive phase, UC's type and dimension, and their transmission magnitude and phase.

SI.	Cell center position along x-axis (mm)	Progressive phase delay (deg.)	Unit cell type	b (type-I) / d (type-II) (mm)	$\lvert S_{21} \rvert$ (dB)	$\angle S_{21}$ (deg.)	Normalize phase $\approx (360\text{-}\angle S_{21})$ (deg.)
1	-46.2	170	type-I	3.99	-0.33	170.5	190
2	-37.8	215	type-I	4.54	-2.25	215.8	145
3	-29.4	260	type-II	3.47	-1.65	259.7	100
4	-21	305	type-II	3.84	-0.18	305.6	55
5	-12.6	350	type-II	4.17	-2.16	349.3	10
6	-4.2	35	type-I	3.24	-1.58	34.1	325
7	4.2	80	type-I	3.38	-0.63	80.1	280
8	12.6	125	type-I	3.64	-0.70	125.4	235
9	21	170	type-I	3.99	-0.33	170.5	190
10	29.4	215	type-I	4.54	-2.25	215.8	145
11	37.8	260	type-II	3.47	-1.65	259.7	100
12	46.2	305	type-II	3.84	-0.18	305.6	55
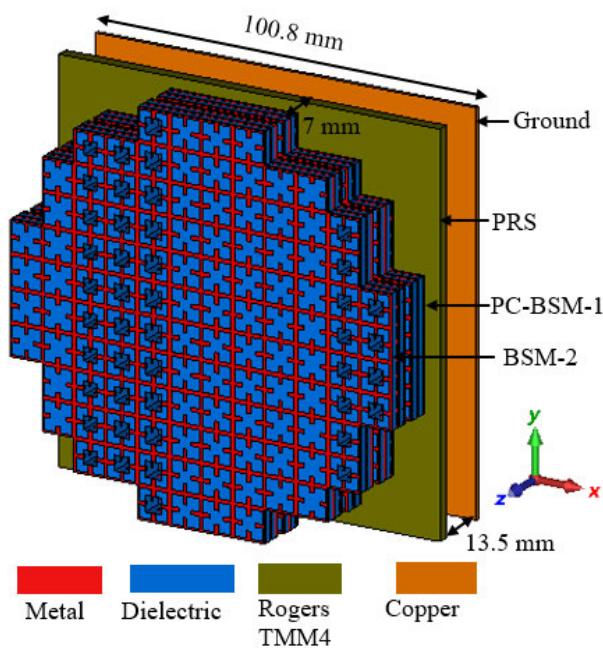
FIGURE 4. Perspective view of the BSM-2 with the whole system.

The minimum transmission magnitude for the cells used in the proposed hybrid metasurface is 2.1 dB with phase coverage ranging from 0° to 360°.

C. BEAM STEERING METASURFACE DESIGN

The BSM-2 is developed by integrating appropriate cells discussed in section III-B. The lateral size of the beam steering metasurface is equal to the aperture of the RCA. To design the linear phase progressive metasurface for beam steering, the aperture of the antenna is virtually divided into a 12×12 square grid with a grid size of 8.4 mm, the same as the unit cell size. According to the antenna phased array theory, the phase gradient of the metasurface should be constant along the y-axis and progressive along the x-axis to steer the beam to an offset angle.

The phase difference between two adjacent cells can be calculated by [1],

$$\Delta\phi = a \times \sin\delta_i \times k_0 \tag{8}$$

where k_0 is the wave number in free space, and 'a' represents the center-to-center distance between two adjacent cells. BSM-2 is designed to tilt the beam by $\delta_2 = 22°$ in off-broadside direction. Using Eq. 8, the phase difference between two adjacent cells should be 45° to tilt the beam to 22°. The absolute value of the phase is not important, but the phase difference ($\Delta\phi$) between any two adjacent cells along the x-axis should be identical. The transmission phase delay of the cells in the leftmost column in the aperture is set to 170°. Then, the phase increases linearly along the x-axis with the step size of 45°. The progressive phases for beam steering, center positions of the cells from left to right along the x-axis, the corresponding cell's dimension that provides the required phase delay, and their transmission magnitude and phase are mentioned in Table 2. Based on the required progressive phase delay, the unit cells are selected to create a highly transparent meta-steering surface. The perspective view of BSM-2 and the whole system are shown in Fig. 4.

D. METASURFACE DESIGN COMBINING PHASE-CORRECTION AND BEAM-STEERING

As the near-field phase distribution of the resonant cavity antenna is not uniform, this non-uniform phase causes poor far-field radiation performance. Before beam steering of the RCA antenna, it is essential to enhance the far-field radiation using the near-field phase correction method for efficient beam steering. The phase-correcting metasurface (PCM) is designed based on the principle of optical ray theory, where the point source is placed at a focal distance from the lens. The details of the phase-correcting metasurface design are available in [36] and [37] and briefly described here. A schematic diagram shown in Fig. 5 describes how a PCM transforms the non-uniform phase of RCA into a more uniform phase. Unlike the lens, the metasurface is placed in the near-field region, usually at a quarter wavelength distance. To design the phase-correcting metasurface, the aperture of the antenna is virtually divided into 12×12 square
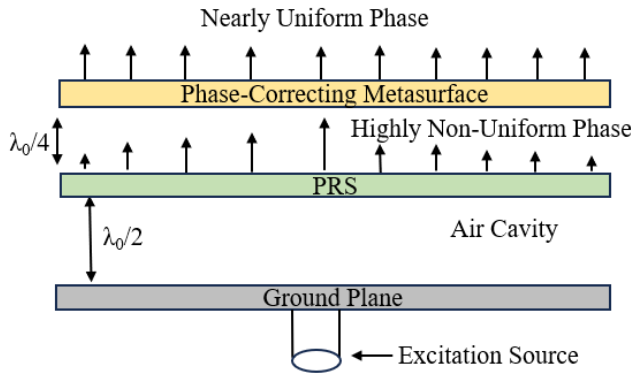
FIGURE 5. Schematic diagram of RCA with phase-correcting metasurface.

TABLE 3. Phase calculation for near-field phase-correcting metasurface design.

SI	Aperture location (along x-axis) (mm)	Probed phase (θ_p)(deg.)	Correction phase delay (200-θ_p) (deg.)
1	4.2	139.85	60.15
2	12.6	109.74	90.26
3	21	67.32	132.68
4	29.4	26.02	173.98
5	37.8	-17.35	217.35
6	46.2	-43.05	243.05

r/c	1	2	3	4	5	6	7	8	9	10	11	12
1					243.1	243.1	243.1	243.1				
2			243.1	243.1	217.4	217.4	217.4	217.4	243.1	243.1		
3		243.1	217.4	217.4	174.0	174.0	174.0	174.0	217.4	217.4	243.1	
4		243.1	217.4	174.0	132.7	132.7	132.7	132.7	174.0	217.4	243.1	
5	243.1	217.4	174.0	132.7	132.7	90.3	90.3	132.7	132.7	174.0	217.4	243.1
6	243.1	217.4	174.0	132.7	90.3	60.2	60.2	90.3	132.7	174.0	217.4	243.1
7	243.1	217.4	174.0	132.7	90.3	60.2	60.2	90.3	132.7	174.0	217.4	243.1
8	243.1	217.4	174.0	132.7	132.7	90.3	90.3	132.7	132.7	174.0	217.4	243.1
9		243.1	217.4	174.0	132.7	132.7	132.7	132.7	174.0	217.4	243.1	
10		243.1	217.4	217.4	174.0	174.0	174.0	174.0	217.4	217.4	243.1	
11			243.1	243.1	217.4	217.4	217.4	217.4	243.1	243.1		
12					243.1	243.1	243.1	243.1				

(a)

r/c	1	2	3	4	5	6	7	8	9	10	11	12
1					233.1	278.1	323.1	8.1				
2			143.1	188.1	207.4	252.4	297.4	342.4	53.1	98.1		
3		98.1	117.4	162.4	164.0	209.0	254.0	299.0	27.4	72.4	143.1	
4		98.1	117.4	119.0	122.7	167.7	212.7	257.7	344.0	72.4	143.1	
5	53.1	72.4	74.0	77.7	122.7	125.3	170.3	257.7	302.7	29.0	117.4	188.1
6	53.1	72.4	74.0	77.7	80.3	95.2	140.2	215.3	302.7	29.0	117.4	188.1
7	53.1	72.4	74.0	77.7	80.3	95.2	140.2	215.3	302.7	29.0	117.4	188.1
8	53.1	72.4	74.0	77.7	122.7	125.3	170.3	257.7	302.7	29.0	117.4	188.1
9		98.1	117.4	119.0	122.7	167.7	212.7	257.7	344.0	72.4	143.1	
10		98.1	117.4	162.4	164.0	209.0	254.0	299.0	27.4	72.4	143.1	
11			143.1	188.1	207.4	252.4	297.4	342.4	53.1	98.1		
12					233.1	278.1	323.1	8.1				

(b)

FIGURE 6. (a) Phase profile for phase correction (b) Phase profile for phase correction and beam steering together.

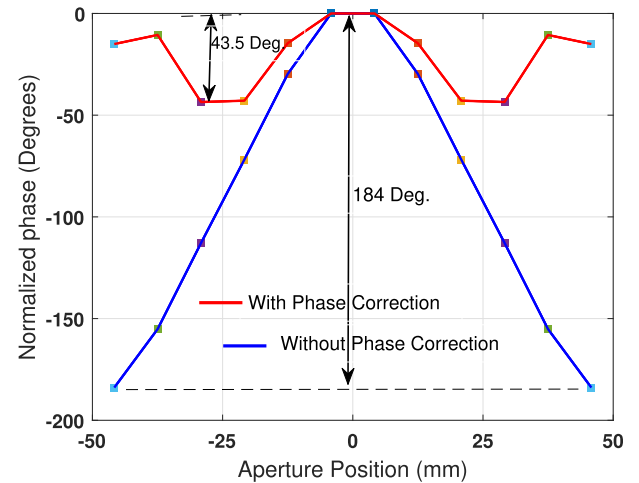**FIGURE 7.** Electric-field (E_y) phase distribution along the x-axis before and after phase correction.

grid with the cell size equal to the unit cell size (8.4 mm) following the process described in [38] and [39].

Then, the phase of the dominant electric field (E_y) is probed at the center of each cell in the grid at a distance of 5 mm ($\approx \lambda_0/5$) using the CST-MWS time-domain solver that is listed in Table 3. To compensate for the non-uniform phase, a reference phase is set to 200°. By subtracting the probed phase of each cell from the reference phase, the required phase delay for each cell is obtained. The near-field phase distribution of an aperture-type antenna can be approximated to exhibit concentric circular symmetry [40], [41]. Therefore, the required phase delay is calculated for only six distinct cells from the center along the x-axis. Each cell's center position, probed phase, and required phase delay are listed in Table 3. The required phase delay profile of the whole aperture for phase correction is shown in Fig. 6. Based on the required phase delay, appropriate unit cells are selected from those discussed in section III-B, and the phase-correcting surface is designed by integrating the unit cells. The electric field phase distribution along the x-axis before and after near-field phase correction is shown in Fig. 7, where the phase error is 184° before phase correction. After phase correction, the phase error is reduced significantly to 43.5°, and far-field radiation is improved due to improvement in phase uniformity.

Two beam steering metasurfaces can be placed on top of the phase-correcting surface for 2D beam steering, but this increases the overall antenna height [25]. The phase-correcting and lower steering surfaces can be merged

to minimize the overall antenna height. This combined surface is called phase-correcting and beam-steering meta-surface (PC-BSM-1). To develop the PC-BSM-1, which provides both phase correction and linear-progressive phase delay for beam steering, the phase delay for phase correction and beam steering are added locally to each cell. Based on

the resultant phase delay, appropriate unit cells are elected to design this metasurface. For example, the phase delay for phase correction of the cells in column 1 in Fig. 6a is 243.1°, while the phase delay for beam steering in the same cell is 170 °. The total normalized phase delay for the cells is 53.1 ° (243.1+170-360). Unit cell type-I with b=3.33 mm is selected to provide this resultant phase delay 53.1 °. Similarly, phase delay for all individual cells is calculated. The whole aperture phase delay profile for the PC-BSM-1 is shown in Fig. 6b. The PC-BSM-1 is designed by choosing and integrating the proper unit cell to provide the required phase delays. A perspective view of PC-BSM-1 is shown in Fig. 8, and it is placed at a distance of 7 mm from the PRS.
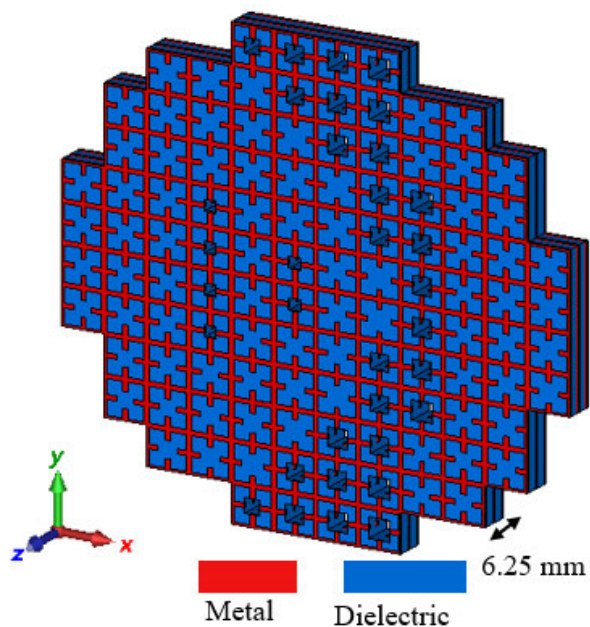

FIGURE 9. Radiation pattern cuts in azimuth plane for different rotation angle (β_2) of BSM-2 from 0° to 180° with a step size of 30°.

FIGURE 10. Directivity with the variation in frequency for different orientations of BSM-2.

FIGURE 8. Perspective view of phase-correcting and beam steering metasurface.

IV. RESULT ANALYSIS

The beam steering system is simulated using a time-domain solver in CST-MWS software to evaluate the performance of the proposed prototype. In our simulation, the dielectric material is defined using measured data (d_k = 4.4, $\tan \delta$ = 0.004) from material characterization reported in [42]. Two cases are considered to demonstrate the efficacy of the proposed metal-dielectric metasurface-based beam steering system with RCA. In case I, PC-BSM-1 is kept stationary, while BSM-2 is rotated from 0° to 180° with a step size of 30° to steer the beam in both the elevation and azimuth plane. In case II, PC-BSM-1 and BSM-2 are rotated synchronously with the same angle but in opposite directions to move the antenna beam in only the elevation plane while the azimuth angle is constant. The results for both cases are discussed in the following subsections.
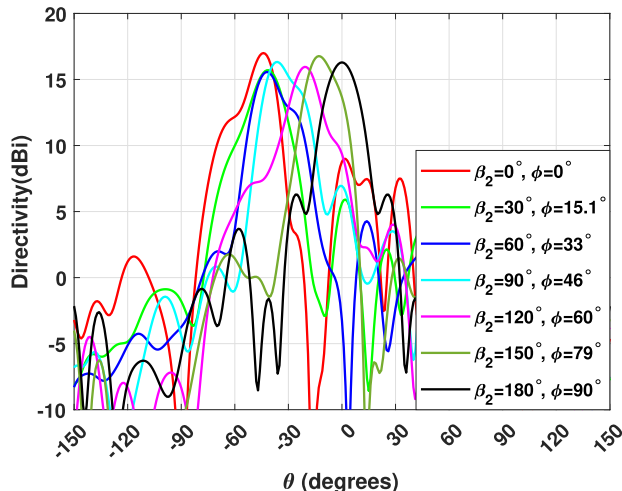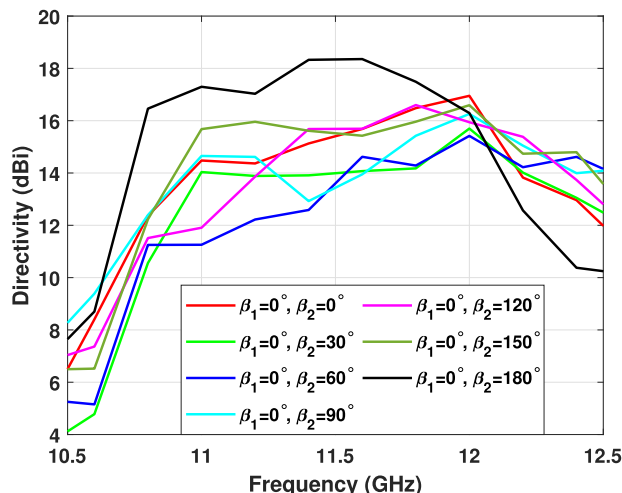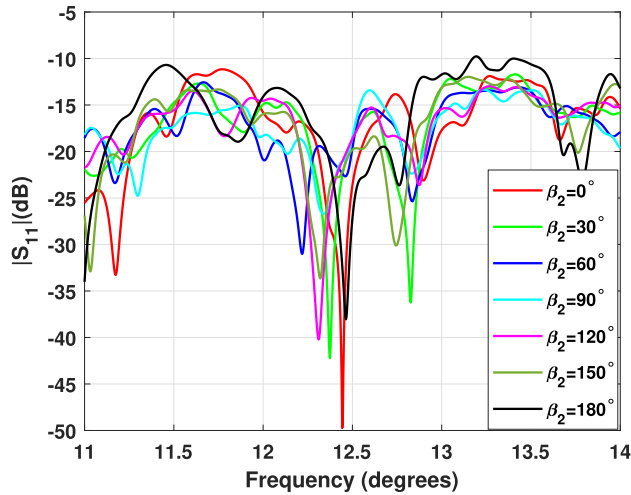
A. CASE-I: BEAM STEERING IN AZIMUTH AND ELEVATION PLANE SIMULTANEOUSLY

In this case, the antenna beam can be steered in both the elevation and azimuth planes by rotating only the BSM-2 and keeping PC-BSM-1 stationary. As an example, BSM-2 is rotated to the angles, $\beta_2 = 0°$, 30°, 60°, 90°, 120°, 150°, and 180°, while $\beta_1 = 0°$. The rotation angles for BSM-2 and their corresponding expected beam directions (θ_s,ϕ_s) from simulation, as well as estimated directions (θ_e,ϕ_e) from theoretical calculations using the paraxial approximation method, are listed in Table 4.

The results show that the expected beam direction from the simulation is more closely aligned with the theoretically calculated direction using the first-order paraxial method than with the results calculated using the phase method, as shown in Table 1. Table 4 indicates that the maximum difference in elevation angle between the simulated and estimated value

TABLE 4. Case-I: Theoretically estimated and simulated beam direction and their corresponding performance when only BSM-2 is rotated.

β_1 (deg.)	β_2 (deg.)	Estimated θ_e (deg.)	Estimated ϕ_e (deg.)	Simulated ϕ_s (deg.)	Simulated ϕ_s (deg.)	Difference $|\theta_e - \theta_s|$	Difference $|\phi_e - \phi_s|$	Peak Directivity (dB)	SLLs (dB)	3-dB Directivity. Bandwidth (%)
0	0	44	0	-44	0	0	0	17	-8	10.4
0	30	42.5	15	-42	15.1	0.5	0.5	15.7	-9.8	12.8
0	60	38.1	30	-42	33	3.9	2.5	15.6	-11.3	12.6
0	90	31.11	45	-36	46	4.89	1.5	16.3	-9.4	10.4
0	120	22	60	-21	60	1	0	16	-11.9	10.5
0	150	11.39	75	-13	79	1.61	4	16.8	-15	13.7
0	180	0	90	0	90	0	0	16.3	-10	10.5

FIGURE 11. Return loss of the beam steering antenna for different orientations (β_2) of the beam steering upper surface.

using the first-order paraxial method is 4.89 ° when BSM-2 is oriented at $\beta_2 = 90°$, while the maximum difference in azimuth angle is 4 ° when the orientation of BSM-2 is $\beta_2 = 150°$. The directivity pattern cuts at 12 GHz for different orientations of BSM-2 are shown in Fig. 9. In this figure, the beam is tilted in the negative direction of θ due to the progressive phase of the metasurface in descending order. The beam is tilted by a maximum of 44 ° off broadside in the elevation plane when both steering surfaces provide maximum phase delays and are in the position without rotation ($\beta_1 = 0, \beta_2 = 0$). The beam moves towards the broadside direction when the BSM-2 is rotated to 180 °. At 12 GHz, maximum directivity (17 dB) is obtained when $\beta_1 = \beta_2 = 0°$, while the lowest directivity is obtained when $\beta_1 = 0°$ and $\beta_2 = 60°$ which is 15.6 dB. The maximum directivity deviation is only 1.4 dB for different orientations of BSM-2 at 12 GHz. The side lobe levels (SLLs) for all orientations are within the acceptable range.

The changes in directivity due to the variations in frequency for different rotation angles of the BSM-2 are shown in Fig. 10. The 3-dB directivity bandwidth for different rotation angles of BSM-2 ranges from 10.4% and 13.7%. Reflection coefficient (S_{11}) of the beam steering system for $\beta_1 = 0°$ and $\beta_2 = 0°, 30°, \ldots 180°$ is shown in Fig. 11.

For all orientations of BSM-2, S_{11} is less than -14 dB, and the 10-dB return loss bandwidth is greater than 25%.

B. IMPACT OF INTER-SPACING BETWEEN PC-BSM-1 AND BSM-2

The distance of PC-BSM-1 from the PRS should not be changed, as this distance is adjusted to provide maximum directivity at the design frequency without placing the beam steering surface in front of the RCA. The impact of the distance between PC-BSM-1 and BSM-2 (d_{BSM-2}) on far-field radiation performance has been investigated when the beam is in the broadside direction ($\beta_1 = 0$, $\beta_2 = 180°$). This spacing varies from $\lambda/16$ to $\lambda/6$, and their corresponding radiation performance is shown in Fig. 12. As d_{BSM-2} increases, the directivity increases (by less than 0.5 dB), and side lobe levels (SLLs) decrease, but not significantly. To lower the overall antenna height, $d_{BSM-2} = 2$ mm $\approx \lambda/12$ is selected as the optimum distance.
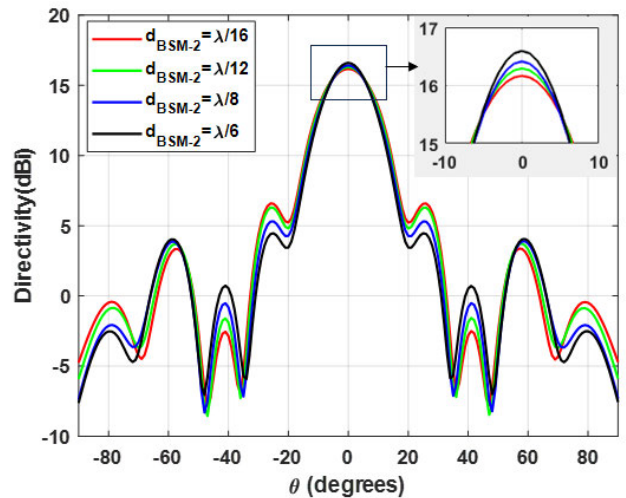

FIGURE 12. Directivity pattern in elevation plane of the beam steering antenna in the broadside direction for inter-spacing variation between PC-BSM-1 and BSM-2 from $\lambda/16$ to $\lambda/6$.

C. CASE-II: BEAM-STEERING IN THE ELEVATION PLANE ONLY BY ROTATING BOTH METASURFACE

The antenna beam can be tilted only in the elevation plane while keeping the azimuth angle fixed by rotating PC-BSM-1 and BSM-2 simultaneously at the same angle but in opposite
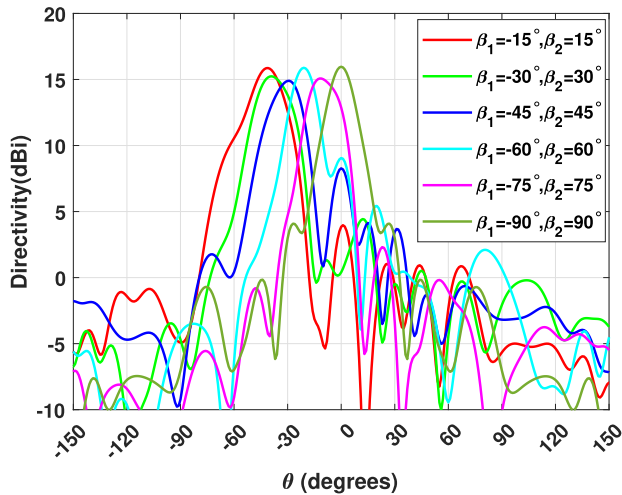
FIGURE 13. Radiations pattern cuts in the azimuth plane at $\phi=0$ when PC-BSM-1 and BSM-2 are rotated at the same angle but in opposite directions.

(a)

(b)

FIGURE 14. Directivity comparison between the results from CST and HFSS software (a) Both surfaces in the position without rotation ($\beta_1 = 0°$, $\beta_2 = 0°$) (b) Upper steering metasurface is rotated, $\beta_2 = 180°$.

directions. In this case, to demonstrate the beam steering efficacy, PC-BSM-1 is rotated clockwise from -15° to -90° in steps of 15°, and BSM-2 is rotated counterclockwise from 15° to 90° with the same step size. The steered beam locations predicted from the full-wave simulation and the estimated beam locations using the paraxial method are listed in Table 5. The difference between the theoretically calculated and predicted results is also mentioned in Table 5. The maximum deviations between them in elevation and azimuth angles are 1.6° and 12.75°, respectively. The power pattern cuts at 12 GHz for different orientations of PC-BSM-1 and BSM-2 are shown in Fig. 13. The beam is tilted the farthest (41°) from broadside in the elevation plane when $\beta_1 = -15°$ and $\beta_2 = 15°$. The beam elevation angle decreases with the increasing rotation angles of both metasurfaces and finally, the beam is directed to the broadside direction when $\beta_1 = -90°$ and $\beta_2 = 90°$.

In this case, the maximum peak directivity (16 dB) is observed in the broadside direction, whereas minimum peak directivity (14.9 dB) is observed when the surfaces are rotated by 45° in the opposite direction. For all orientations of the steering surfaces, the SLLs are lower than -10 dB except for the rotation angles of 45° and 60°. The maximum deviation in directivity is only 1.1 dB across all orientations of the beam steering metasurfaces. Additionally, for all orientations of PC-BSM-1 and BSM-2, the 10-dB impedance matching bandwidth is greater than 25%, and the 3-dB directivity bandwidth is greater than 10%. It is important to mention that the experimental results should be closely aligned with the simulation results based on the fabrication accuracy of the 3-D printing.

To validate the simulation results obtained from the CST software, we have simulated two configurations of our prototype using commercial high-frequency structure simulator (HFSS) software, and their results are shown in Fig. 14. Fig. 14a shows the directivity comparison between the results
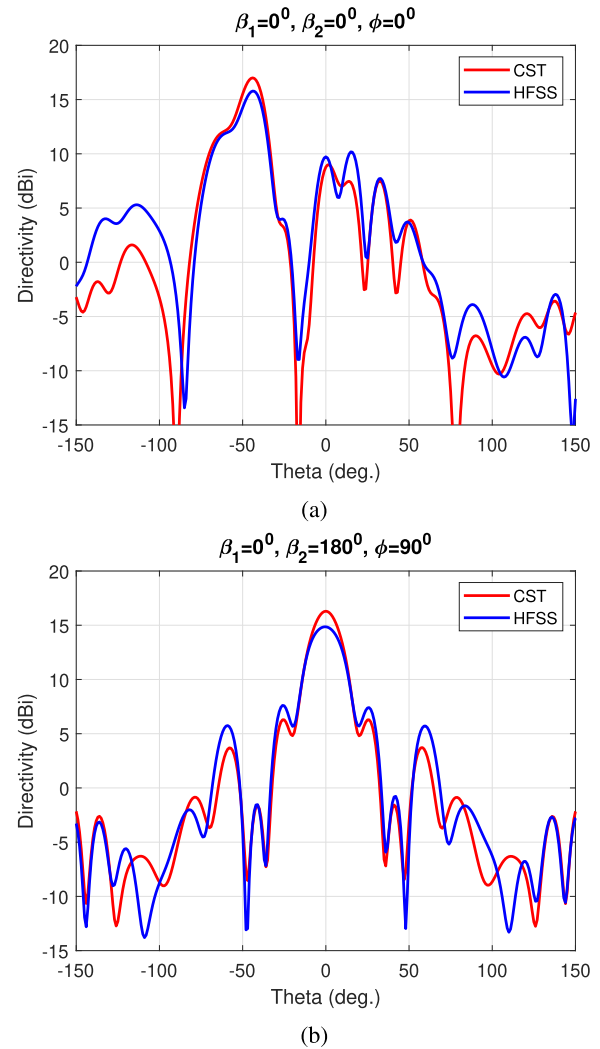
of CST and HFSS when both metasurfaces are in the initial position without rotation. With this configuration of the beam steering system, the beam is steered to a maximum angle (44°). Fig. 14b shows the directivity pattern using both software when the only upper steering metasurface (BSM-2) is rotated 180°. In this configuration, the beam is directed in the broadside direction (0°). From these two figures, it is seen that there is a good alignment between the results from both software. There is a small difference in magnitude due to different numerical calculation methods and divergence accuracy of the two software.

The performance of the proposed metasurface-based beam-steering system is compared with other works reported in the literature, as shown in Table 6. In this table, it is important to mention that the superscript ∗ and + with the reference number represent the articles with simulation and measurement data, respectively. In [2], [20], [21], [25], and [43], there is a good agreement between the simulation and measurement data. The thickness of the proposed

TABLE 5. Case-II: comparison between predicted and theoretically calculated beam steering angles and performance results.

β_1 (deg.)	β_2 (deg.)	Estimated θ_e(deg.)	Estimated ϕ_e(deg.)	Simulated θ_s(deg.)	Simulated ϕ_s(deg.)	Difference $|\theta_e\text{-}\theta_s|$	Difference $|\phi_e\text{-}\phi_s|$	Peak Directivity(dB)	SLLs (dB)	3-dB Directivity Bandwidth(%)
-15	15	42.5	0	-41	-1.5	1.5	1.5	15.9	-11.9	12.98
-30	30	38.1	0	-39	0	0.9	0	15.24	-10.8	10.29
-45	45	31.1	0	-29.5	-6	1.6	6	14.9	-6.6	11.15
-60	60	22	0	-21	0	1	0	15.9	-6.8	11
-75	75	11.38	0	-11.38	-12.75	0	12.75	15.1	-12.8	12
-90	90	0	0	0	0	0	0	16	-11.9	12

TABLE 6. Comparison of the proposed system with state-of-the-art works.

Reference	Operating Frequency (GHz)	Feed Antenna & Steering Method	MS/PT Types & Technology	MS/PT Thickness (λ_0)	Peak Gain (dBi)	Maximum Steering El/Az (deg.)	MS/PT Aperture Size (λ_0)	Max. Aperture Efficiency (%)
This work*	12	WR75 NFMS	Composite, 3-D Printed Single Filament	0.25	15.86	±44/360	4	24
[27]* IEEE OJAP	11	Patch Array NFMS	Composite, 3-D Printed Single Filament	0.36	19.9	±57/360	6	21.56
[19]* IEEE EuCAP	20	Patch NFMS	Printed patch PCB	0.22	16.6	±50/360	6	21.56
[25]+ IEEE Access	11	Horn NFMS	Dielectric, 3-D Printed Single Filament	1.76	15.4	±36/360	4.2	19.7
[2]+ IEEE Access	30	WR28 NFMS	Dielectric, 3-D Printed, Single Filament	3.19	16	±39/360	6	11.21
[20]+ IEEE TAP	34.5	Horn NFMS	Dielectric, 3-D Printed Multiple Filaments	0.51	21.6	±54/360	5.9	42
[43]+ IEEE TAP	9.375	Horn TA-PR	All-Metal, Laser-Cut	0.94	-	±20/360	8	-
[21]+ IEEE TAP	12.5	Horn NFMS	All-Metal, Laser-Cut	0.8	16	±42/360	6	11.21

NFMS – Near-Field Meta-Steering, RCA – Resonant Cavity Antenna, PCB – Printed Circuit Board, Directivity, MS/PT – Metasurface/Phase Transformer, El/Az - Elevation/Azimuth, IEEE TAP – IEEE Transactions on Antennas and Propagation, IEEE OJAP - Open Journal Of Antennas And Propagation, EuCAP - European Conference on Antennas and Propagation, '–' data is unavailable, ∗ – Simulated data, + – Measured data

metasurface is the lowest (only $0.25\lambda_0$) compared to others except [19] where multiple layer-based PCB metasurface was used, increasing the loss. A thinner profile metasurface is beneficial for compact, lightweight applications where minimizing physical space is crucial, such as in satellite communications. The peak gain of the system is slightly lower due to the smaller size of the aperture and the inherent characteristics of RCA. The aperture efficiency is higher than others except [20], where the height of the metasurface is almost double that of the proposed metasurface in this paper. The beam steering range of the proposed system is 360° in the azimuth plane and 88° in the elevation plane, which is higher than that of others except [19], [20], [27]. Comparing the thickness and aperture size of the metasurface, the proposed beam steering system is better with comparable performance.

V. CONCLUSION

A metal-dielectric phase-gradient metasurface-based beam-steering system is presented for the 2-D beam steering applications with the RCA. Comparative analysis with state-of-the-art literature shows that the proposed metasurfaces have the lowest profile and can be fabricated using a multi-material 3-D printer with dielectric and metal using the latest additive manufacturing technology. The 3-D-printed metasurface obviates the challenges associated with conventional manufacturing processes. Near-field phase correction is also included in the bottom metasurface to improve the non-uniform near-field phase and enhance far-field radiation performance. The proposed beam steering system with the RCA can tilt the radiated beam within a conical region with an apex angle of 88° with only a 1.4 dB deviation in directivity. The proposed metasurfaces can be realized using RF-graded, commercially available 3-D printed filaments and metal with a 3-D metal-dielectric printer for optimal performance. The proposed prototype is scalable and reproducible for mass production. Hence, it can be designed at a higher frequency based on the fabrication accuracy of 3-D printing and material characteristics.

REFERENCES

[1] M. Akbari, M. Farahani, A. Ghayekhloo, S. Zarbakhsh, A.-R. Sebak, and T. A. Denidni, "Beam tilting approaches based on phase gradient surface for mmWave antennas," IEEE Trans. Antennas Propag., vol. 68, no. 6, pp. 4372–4385, Jun. 2020.

[2] M. U. Afzal, L. Matekovits, K. P. Esselle, and A. Lalbakhsh, "Beam-scanning antenna based on near-electric field phase transformation and refraction of electromagnetic wave through dielectric structures," *IEEE Access*, vol. 8, pp. 199242–199253, 2020.

[3] A. Dreher, N. Niklasch, F. Klefenz, and A. Schroth, "Antenna and receiver system with digital beamforming for satellite navigation and communications," *IEEE Trans. Microw. Theory Techn.*, vol. 51, no. 7, pp. 1815–1821, Jul. 2003.

[4] K. W. Linnes, W. D. Merrick, and R. Stevens, "Ground antenna for space communication system," *IRE Trans. Space Electron. Telemetry*, vols. SET–6, no. 1, pp. 45–54, Mar. 1960.

[5] R. J. Mailloux, "Phased array theory and technology," *Proc. IEEE*, vol. 70, no. 3, pp. 246–291, 1982.

[6] A. V. Shishlov, "Vehicular antennas for satellite communications," in *Proc. 8th Int. Conf. Antenna Theory Techn.*, Sep. 2011, pp. 34–39.

[7] S. Han, I. Chih-Lin, Z. Xu, and S. Wang, "Reference signals design for hybrid analog and digital beamforming," *IEEE Commun. Lett.*, vol. 18, no. 7, pp. 1191–1193, Jul. 2014.

[8] B. A. F. Esmail, S. Koziel, and S. Szczepanski, "Overview of planar antenna loading metamaterials for gain performance enhancement: The two decades of progress," *IEEE Access*, vol. 10, pp. 27381–27403, 2022.

[9] K. Singh, F. Ahmed, and K. Esselle, "Electromagnetic metasurfaces: Insight into evolution, design and applications," *Crystals*, vol. 12, no. 12, p. 1769, Dec. 2022.

[10] B. A. F. Esmail and S. Koziel, "Design and optimization of metamaterial-based highly-isolated MIMO antenna with high gain and beam tilting ability for 5G millimeter wave applications," *Sci. Rep.*, vol. 14, no. 1, p. 3203, Feb. 2024.

[11] X. Yang, E. Wen, D. Bharadia, and D. F. Sievenpiper, "Multifunctional metasurface: Simultaneous beam steering, polarization conversion, and phase offset," *IEEE Trans. Antennas Propag.*, vol. 72, no. 5, pp. 4589–4593, May 2024.

[12] J. Yu, W. Jiang, and S. Gong, "Low-RCS beam-steering antenna based on reconfigurable phase gradient metasurface," *IEEE Antennas Wireless Propag. Lett.*, vol. 18, no. 10, pp. 2016–2020, 2019.

[13] Y.-H. Lv, X. Ding, B.-Z. Wang, and D. E. Anagnostou, "Scanning range expansion of planar phased arrays using metasurfaces," *IEEE Trans. Antennas Propag.*, vol. 68, no. 3, pp. 1402–1410, Mar. 2020.

[14] B. A. F. Esmail and S. Koziel, "Design and optimization of metamaterial-based 5G millimeter wave antenna for gain enhancement," *IEEE Trans. Circuits Syst. II, Exp. Briefs*, vol. 70, no. 9, pp. 3348–3352, Sep. 2023.

[15] T. Hongnara, S. Chaimool, P. Akkaraekthalin, and Y. Zhao, "Design of compact beam-steering antennas using a metasurface formed by uniform square rings," *IEEE Access*, vol. 6, pp. 9420–9429, 2018.

[16] B. A. F. Esmail, S. Koziel, and A. Pietrenko-Dabrowska, "Design and optimization of a compact super-wideband MIMO antenna with high isolation and gain for 5G applications," *Electronics*, vol. 12, no. 22, p. 4710, Nov. 2023.

[17] M. U. Afzal and K. P. Esselle, "Steering the beam of medium-to-high gain antennas using near-field phase transformation," *IEEE Trans. Antennas Propag.*, vol. 65, no. 4, pp. 1680–1690, Apr. 2017.

[18] K. Singh, M. U. Afzal, M. Kovaleva, and K. P. Esselle, "Controlling the most significant grating lobes in two-dimensional beam-steering systems with phase-gradient metasurfaces," *IEEE Trans. Antennas Propag.*, vol. 68, no. 3, pp. 1389–1401, Mar. 2020.

[19] M. I. Nabeel, M. U. Afzal, D. N. Thalakotuna, and K. P. Esselle, "Beam steering 2D leaky wave resonant cavity antenna for Ka-band satellite communication," in *Proc. 18th Eur. Conf. Antennas Propag. (EuCAP)*, Mar. 2024, pp. 1–5.

[20] A. A. Baba, R. M. Hashmi, M. Attygalle, K. P. Esselle, and D. Borg, "Ultrawideband beam steering at mm-wave frequency with planar dielectric phase transformers," *IEEE Trans. Antennas Propag.*, vol. 70, no. 3, pp. 1719–1728, Mar. 2022.

[21] F. Ahmed, M. U. Afzal, T. Hayat, K. P. Esselle, and D. N. Thalakotuna, "A near-field meta-steering antenna system with fully metallic metasurfaces," *IEEE Trans. Antennas Propag.*, vol. 70, no. 11, pp. 10062–10075, Nov. 2022.

[22] F. Ahmed, M. U. Afzal, K. Singh, T. Hayat, and K. P. Esselle, "Highly transparent fully metallic 1-bit coding metasurfaces for near-field transformation," in *Proc. 16th Eur. Conf. Antennas Propag. (EuCAP)*, Mar. 2022, pp. 1–4.

[23] A. A. Baba, R. M. Hashmi, K. P. Esselle, M. Attygalle, and D. Borg, "A millimeter-wave antenna system for wideband 2-D beam steering," *IEEE Trans. Antennas Propag.*, vol. 68, no. 5, pp. 3453–3464, May 2020.

[24] M. Li, Y. Yang, F. Iacopi, J. Nulman, and S. Chappel-Ram, "3D-printed low-profile single-substrate multi-metal layer antennas and array with bandwidth enhancement," *IEEE Access*, vol. 8, pp. 217370–217379, 2020.

[25] T. Hayat, M. U. Afzal, F. Ahmed, S. Zhang, K. P. Esselle, and J. Vardaxoglou, "The use of a pair of 3D-printed near field superstructures to steer an antenna beam in elevation and azimuth," *IEEE Access*, vol. 9, pp. 153995–154010, 2021.

[26] *PREPERM^{TM}*. (2024). *Preperm Materials Website*. Accessed: Jan. 19, 2024. [Online]. Available: https://www.avient.com/products/engineered-polymer-formulations/conductive-signal-radiation-shielding-formulations/preperm-low-loss-dielectric-thermoplastics

[27] F. Ahmed, T. Hayat, M. U. Afzal, S. Zhang, K. P. Esselle, and W. G. Whittow, "3-D printable synthetic metasurface to realize 2-D beam-steering antenna," *IEEE Open J. Antennas Propag.*, vol. 4, pp. 506–519, 2023.

[28] Y. Lu, Y. Zhou, M. Hei, and D. Fan, "Theoretical and experimental determination of steering mechanism for Risley prism systems," *Appl. Opt.*, vol. 52, no. 7, pp. 1389–1398, 2013.

[29] J. Wang and Y. Ramhat-Samii, "Phase method: A more precise beam steering model for phase-delay metasurface based Risley antenna," in *Proc. URSI Int. Symp. Electromagn. Theory (EMTS)*, May 2019, pp. 1–4.

[30] F. Ahmed, M. U. Afzal, T. Hayat, K. P. Esselle, and D. N. Thalakotuna, "A dielectric free near field phase transforming structure for wideband gain enhancement of antennas," *Sci. Rep.*, vol. 11, no. 1, p. 14613, Jul. 2021.

[31] S. Shrestha, S. M. Abbas, M. Asadnia, and K. P. Esselle, "Realization of three dimensional printed multi layer wide band prototype," *IEEE Access*, vol. 10, pp. 130944–130954, 2022.

[32] M. Abdullah and S. Koziel, "Supervised-learning-based development of multibit RCS-reduced coding metasurfaces," *IEEE Trans. Microw. Theory Techn.*, vol. 70, no. 1, pp. 264–274, Jan. 2022.

[33] A. Lalbakhsh, M. U. Afzal, K. P. Esselle, and S. L. Smith, "Low-cost nonuniform metallic lattice for rectifying aperture near-field of electromagnetic bandgap resonator antennas," *IEEE Trans. Antennas Propag.*, vol. 68, no. 5, pp. 3328–3335, May 2020.

[34] P. Xie, G. Wang, H. Li, and X. Gao, "A novel methodology for gain enhancement of the Fabry–Pérot antenna," *IEEE Access*, vol. 7, pp. 176170–176176, 2019.

[35] K. Singh, M. U. Afzal, and K. P. Esselle, "Accurate optimization technique for phase-gradient metasurfaces used in compact near-field meta-steering systems," *Sci. Rep.*, vol. 12, no. 1, p. 4118, Mar. 2022.

[36] M. U. Afzal, K. P. Esselle, and B. A. Zeb, "Dielectric phase-correcting structures for electromagnetic band gap resonator antennas," *IEEE Trans. Antennas Propag.*, vol. 63, no. 8, pp. 3390–3399, Aug. 2015.

[37] M. Y. Ali, A. Lalbakhsh, S. Koziel, L. Golunski, F. Ahmed, and M. Asadnia, "A low-profile 3-D printable metastructure for performance improvement of aperture antennas," *Sci. Rep.*, vol. 14, no. 1, p. 17930, Aug. 2024.

[38] T. Hayat, M. U. Afzal, A. Lalbakhsh, and K. P. Esselle, "Additively manufactured perforated superstrate to improve directive radiation characteristics of electromagnetic source," *IEEE Access*, vol. 7, pp. 153445–153452, 2019.

[39] A. Lalbakhsh, M. U. Afzal, and K. P. Esselle, "Multiobjective particle swarm optimization to design a time-delay equalizer metasurface for an electromagnetic band-gap resonator antenna," *IEEE Antennas Wireless Propag. Lett.*, vol. 16, pp. 912–915, 2017.

[40] A. Lalbakhsh, M. U. Afzal, K. P. Esselle, and S. L. Smith, "Wideband near-field correction of a Fabry–Pérot resonator antenna," *IEEE Trans. Antennas Propag.*, vol. 67, no. 3, pp. 1975–1980, Mar. 2019.

[41] F. Ahmed, M. U. Afzal, T. Hayat, K. P. Esselle, and D. N. Thalakotuna, "Self-sustained rigid fully metallic metasurfaces to enhance gain of shortened horn antennas," *IEEE Access*, vol. 10, pp. 79644–79654, 2022.

[42] S. Zhang, R. K. Arya, W. G. Whittow, D. Cadman, R. Mittra, and J. C. Vardaxoglou, "Ultra-wideband flat metamaterial GRIN lenses assisted with additive manufacturing technique," *IEEE Trans. Antennas Propag.*, vol. 69, no. 7, pp. 3788–3799, Jul. 2021.

[43] X. Zhao, C. Yuan, L. Liu, S. Peng, Q. Zhang, L. Yu, and Y. Sun, "All-metal beam steering lens antenna for high power microwave applications," *IEEE Trans. Antennas Propag.*, vol. 65, no. 12, pp. 7340–7344, Dec. 2017.

MD YEAKUB ALI (Student Member, IEEE) received the B.Sc. degree in engineering from the Department of Electronics and Telecommunication Engineering (ETE), Rajshahi University of Engineering and Technology (RUET), Rajshahi, Bangladesh, in 2014, and the M.Sc. degree in engineering from the Department of Electrical and Electronic Engineering (EEE), RUET, in 2020. He is currently pursuing the Ph.D. degree with the School of Engineering, Macquarie University, Sydney, NSW, Australia. He was an Engineer with Bangla Trac Communication and Robi Axiata Ltd., from 2014 to 2017. He was a Lecturer with the Department of ETE, RUET, from 2017 to 2021, and promoted to an Assistant Professor in 2021, and on leave for higher study (Ph.D.). His research interests include antennas for mobile and satellite communication and metasurfaces for antenna applications.

KHUSHBOO SINGH (Member, IEEE) received the Bachelor of Technology degree (Hons.) in electronics and communication engineering from SHIATS, India, the Master of Science (by Research) degree in electronics and communication engineering from LNMIIT, India, and the Ph.D. degree in electrical engineering from Macquarie University, Australia, focusing on antenna and propagation research. She is a Research Fellow with the University of Technology Sydney. Formerly, she was an Associate Professor, a Guest Lecturer, and a Casual Academic, teaching undergraduate courses mostly in antenna, electromagnetics, and microwave engineering. Two main themes that best summaries her current postdoctoral research endeavors are high-gain, beam-steering antennas, and mm-wave high-power planar array antennas. In addition, she is developing reconfigurable intelligent surfaces (RIS) and metasurfaces. She is actively involved in cutting-edge research and collaborates on critical projects with the Defence Science and Technology Group and the NSW government. The Australian government supported her Ph.D. studies via the acclaimed iRTP scholarship initiative. Her master's degree research emphasis on radio-frequency (RF) front-end components, funded by a merit-based LNMIIT Scholarship. In addition to her degree scholarships, she has received several grants and fellowships. Her achievements include a successful Blue-Sky Research Grant (2022–2023); the Australia-India Research Student Fellowship, in 2023; and the Early Career Researcher (ECR) Capability Development Grant, in 2024. She bagged the ChooseMaths grant from the Australian Mathematical and Statistical Institute, in 2017. She also received the grant for a five-month internship under the Australian Postgraduate Research Intern (APR) Program. She received the Silver Medal during the bachelor's degree. Her significant contributions to the DSTG Project earned her team MetaSteerers, the 2023 Eureka Prize for Outstanding Science for Safeguarding Australia. In 2020, she was announced as an Outstanding Reviewer for IEEE TRANSACTIONS ON ANTENNAS AND PROPAGATION.

ALI LALBAKHSH (Senior Member, IEEE) received the B.S. and M.S. degrees in electronic and telecommunication engineering, in 2008 and 2011, respectively, and the H.D. and Ph.D. degrees in electronics engineering from Macquarie University, Australia, in 2015 and 2020, respectively. He is an Academic Researcher (Macquarie University Research Fellowship) with Macquarie University. He has published over 120 peer-reviewed journals and conference papers. His research interests include satellite communication, high-gain antennas, evolutionary optimization methods, and passive microwave components. He received several prestigious awards, including the International Research Training Program Scholarship (iRTP) for the MRes, the International Macquarie University Research Excellence Scholarship (iMQRES) for the Ph.D. degree, the Commonwealth Scientific and Industrial Research Organization (CSIRO) grants on Astronomy and Space Exploration, the Macquarie University Postgraduate Research Fund (PGRF), and the WiMed Travel Support Grants. He was a recipient of the 2016 ICEAA-IEEE APWC Cash Prize and the Macquarie University Deputy Vice-Chancellor Commendation, in 2017. He is a Researcher in the IEEE Region 10 (Asia–Pacific) and has received the Most Prestigious Best Paper Contest of the IEEE Region 10, for many times. He received the third prize, the first prize, and the second prize from the international competition, in 2016, 2018, and 2019, respectively. He was highly commended as a finalist and the winner of the Excellence in Higher Degree Research Award in Science, Technology, Engineering, Mathematics and Medicine (STEMM), Macquarie University, in 2019 and 2020, respectively. In 2020, he was announced as an Outstanding Reviewer of IEEE TRANSACTIONS ON ANTENNAS AND PROPAGATION; and received the Research Excellence Award of the Faculty of Science and Engineering, Macquarie University. He serves as an Associate Editor for *International Journal of Electronics and Communications* and *Electronics* (MDPI).

SLAWOMIR KOZIEL (Fellow, IEEE) received the M.Sc. and Ph.D. degrees in electronic engineering from Gdańsk University of Technology, Poland, in 1995 and 2000, respectively, and the M.Sc. degree in theoretical physics and the M.Sc. and Ph.D. degrees in mathematics from the University of Gdańsk, Poland, in 2000, 2002, and 2003, respectively. He is currently a Professor with the Department of Engineering, Reykjavik University, Iceland. His current research interests include the CAD and modeling of microwave and antenna structures, simulation-driven design, surrogate-based optimization, space mapping, circuit theory, analog signal processing, evolutionary computation, and numerical analysis.

LUKASZ GOLUNSKI received the M.Sc. degree in materials engineering and the Ph.D. degree in electronic engineering from Gdańsk University of Technology, Poland, in 2011 and 2018, respectively. He is currently an Assistant Professor with the Faculty of Electronics, Telecommunications and Informatics, Gdańsk University of Technology. His research interests include thin film growth, chemical vapor deposition and physical vapor methods, semiconductor diamond synthesis, and their electrical analysis.

• • •